Modelling the effect of non-uniform radon progeny activities on transformation frequencies in human bronchial airways

H. Fakir, W. Hofmann, Isabelle Aubineau-Lanièce

MODELLING THE EFFECT OF NON-UNIFORM RADON PROGENY ACTIVITIES ON TRANSFORMATION FREQUENCIES IN HUMAN BRONCHIAL AIRWAYS

H. FAKIR[1], W. HOFMANN[1], I. AUBINEAU-LANIECE[2]

[1]Division of Physics and Biophysics, Department of Material Science, University of Salzburg, Salzburg, Austria

[2]Institut de Radioprotection et de Sûreté Nucléaire (IRNS), DRPH/SDI, Fontenay-aux-Roses, France

Corresponding Author:

Hatim Fakir, PhD
Division of Physics and Biophysics
Department of Material Science
University of Salzburg
Hellbrunner Str. 34
A-5020 Salzburg, Austria
Tel: ++ 43-662-8044-5709
Fax: ++43-662-8044-150
E-mail: hatim.fakir@sbg.ac.at

ABSTRACT

The effects of radiological and morphological source heterogeneities in straight and Y-shaped bronchial airways on hit frequencies and microdosimetric quantities in epithelial cells have previously been investigated. The goal of the present study is to relate these physical quantities to transformation frequencies in sensitive target cells and to radon-induced lung cancer risk. Based on an effect specific track length model, computed linear energy transfer (LET) spectra were converted to corresponding transformation frequencies for different activity distributions and source-target configurations. Average transformation probabilities were considerably enhanced for radon progeny accumulations and target cells at the carinal ridge, relative to uniform activity distributions and target cells located along curved and straight airway portions at the same exposure level. While uncorrelated transformations probabilities produce a linear dose-effect relationship, correlated transformations first increase depending on LET, but then drop significantly when exceeding a defined number of hits or cumulative exposure level.

Keywords: radon progeny, alpha particles, microdosimetry, human lung, airway bifurcation, oncogenic transformation, lung cancer risk

INTRODUCTION

Current lung cancer risk assessments for the inhalation of short-lived radon progeny are based on dosimetric models that assume a uniform distribution of the activity within infinitely long cylinders[1-7]. However, several experimental and theoretical studies of particle deposition in human airways indicated a strong inhomogeneity of the radon progeny deposition pattern in bronchial airway bifurcations, with significantly enhanced deposition at the carinal ridge[8-13]. Thus enhanced deposition and reduced mucociliary clearance at carinal ridges will yield much higher radiation doses in sensitive target cells located at such sites relative to a uniform surface activity distribution[8, 11-13]. Furthermore, neoplastic and preneoplastic lesions were preferentially observed at the carinal ridges in histological studies[14, 15], suggesting that bronchial tumors are preferentially initiated within bronchial airway bifurcations.

Recently, a Monte Carlo code has been developed to calculate microdosimetric quantities for uniform and non-uniform distributions of the surface activities of alpha-emitting radon progeny in cylindrical airways[16] and bifurcation regions[17]. This code was applied to the analyses of the impact of radiological and morphological source heterogeneities in straight and Y-shaped bronchial airways on cellular dosimetric quantities, such as absorbed dose, hit frequency, lineal energy, single hit and dose-dependent specific energy. These simulations demonstrated that cellular dose quantities for non-uniformly distributed surface activities exhibit significant variations, as high as several orders of magnitude, for cells located at different sites within a bifurcation and at different depths in bronchial epithelium.

The question then arises about the biological significance of these non-uniform surface activity patterns and their relevance for lung cancer incidence. In other words, can the observed variations of microdosimetric quantities illustrating the non-uniform radon progeny surface

activities be related to corresponding variations of cellular biological radiation effects relevant for carcinogenesis, such as oncogenic transformation? Thus the goal of this paper is to convert microdosimetric spectra to transformation frequencies on the basis of a modified formulation of the probability-per-unit-track-length (PPUTL) model for inactivation and oncogenic transformation[18-20] for different activity distributions and airway geometries.

The microdosimetric approach adopted here refers to energy deposition and resulting biological effects in single cells or cell nuclei. Thus the present analysis is made for selected epithelial cells rather than averaging over the entire airway wall structure as it is commonly done in average dose based approaches. To relate the transformation probabilities computed in this paper to the earlier simulations of microdosimetric quantities in cylindrical airways[16] and airway bifurcations[17], the same source-target geometries and target cell locations were assumed.

MICRODOSIMETRIC MODEL

The Monte Carlo code used in the present study was developed for the simulation of microdosimetric spectra for uniform and non-uniform alpha-emitting radionuclide distributions in straight cylindrical and Y-shaped airway bifurcations[16,17,21]. For the inhalation of short-lived radon decay products, alpha particles are emitted from ^{214}Po and ^{218}Po with energies of 7.69 and 6.0 MeV and ranges in tissues of about 72 and 47 μm, respectively. This code calculates alpha particle energy and microdosimetric spectra in cell nuclei located at given sites, based on the continuous slowing down approximation (CSDA). Dosimetric quantities computed by the code are: absorbed dose, hit frequency, lineal energy spectra, single hit and dose-dependent specific energy spectra, linear energy transfer (LET) spectra, and quality factor. The fundamental quantity characterizing the source - target geometry is the hit probability. Hit frequencies are then

obtained by multiplying the computed hit probabilities by the activity or the number of alpha particles emitted by the ^{218}Po and ^{214}Po nuclides from the considered source volume. Consequently, the microdosimetric spectra were normalized to the total number of hits in a given target cell.

Radiation energy and quality in oncogenic transformation experiments is commonly described by the LET of the incident radiation. Consequently, the probabilities per unit track lengths derived from in vitro experiments are expressed as functions of LET. For the energies and the target size considered in the present study, LET is a suitable approximation of the energy loss along alpha particles tracks[22]. Hence LET distributions and their related track averages are used to illustrate the variability of energy deposition as a result of inhomogeneous activity distributions.

BIOPHYSICAL MODEL

The probability-per-unit-track-length (PPUTL) biophysical model has been developed to relate energy deposition by random alpha particle track lengths through target cell nuclei with experimentally observed in vitro biological endpoints like inactivation, oncogenic transformation, and mutation. Since the model has been described in detail in previous reports[18-20], only its modifications for the present study will be described here.

The probabilities per unit track length as a function of the LET (L) for hitting a target in the cell nucleus related to oncogenic transformation, $P_T(L)$, and cell inactivation, $P_D(L)$, were derived from experimental studies on the C3H 10T1/2 cells[23]. If T is the track length of an alpha particle traversing the target cell nucleus and L its LET, the quantities $P_T(L)\times T$ and $P_D(L)\times T$ represent the total probabilities for hitting targets within the cell nucleus related to transformation

and inactivation of the cell. In previous reports[20,24], oncogenic transformations for uniformly distributed activities and low level exposures (hit frequencies <1) were calculated by integrating over the LET and the track length distributions. However, for non-uniformly distributed activities and for high exposure levels, cell nuclei may experience multiple alpha traversals. Hence to investigate the effect of non-uniform activities on oncogenic transformation, the PPUTL model was modified to consider the number of hits actually received by the target nuclei and the potential correlation between individual hits. Predictions of the revised model agree well with the experimental observations of micro-beam experiments by Miller et al.[25,26]. In the present work, a subroutine was implemented into the microdosimetric code to calculate for each randomly obtained LET, L, and track length, T, the quantities $P_T(L)\times T$ and $P_D(L)\times T$. The conditional probabilities that an individual cell is transformed and survives, $P_{TS}(L,T)$, were then calculated using the following equation:

$$P_{TS}(L,T)=\left[\sum_{i=0}^{m-1}\frac{\left(P_D(L)\times T\right)^i}{i!}\cdot\exp\left(-P_D(L)\times T\right)\right]\times\left[1-\sum_{i=0}^{n-1}\frac{\left(P_T(L)\times T\right)^i}{i!}\cdot\exp\left(-P_T(L)\times T\right)\right] \quad (1)$$

The first and the second term, respectively, represent the surviving and the transformation probabilities, and m and n are the numbers of targets to be hit to induce cell inactivation and transformation, which are set equal to 2[20].

For low level exposures, where the number of hits is smaller than 1, individual particle tracks are assumed to act independently and the transformation probabilities for single hits are normalized to the hit frequency. However, when the cells experience multiple hits, single cell traversals may be correlated to each other and induce more complicated transformation-inactivation combinations. Thus modeling multiple traversal correlations should account for the

lag time between different particle traversals, the cell cycle time, the dynamics of cell repair mechanisms, and the potential occurrence of bystander effects and genomic instability.

For the analysis of radiation-induced lung cancer, Leenhouts and Chadwick[27] proposed that in an acute radiation exposure, total dose is the relevant quantity which determines cellular radiation effects. In a protracted exposure, however, the crucial radiation quantity for cellular effects is the dose per cell cycle[28]. Thus calculations for low chronic exposures were made for cells during an average cell cycle time of 30 days[3,29] and cells in that same location, but at different times, are assumed to be independently affected. In terms of cellular hits, both acute and protracted exposures are represented here by two extreme cases bracketing all possible exposure scenarios from chronic low level residential exposure to short-term high occupational exposure in uranium mines:

i) No correlation between the hits: The transformation probability per surviving cell is calculated by adding up the total probabilities per surviving cell for each traversal independently. This assumption is valid for very low hit frequencies or for multiple hits supposed to be distant enough in time (regarding repair mechanisms and genomic instability) to be considered as independent events.

ii) Total correlation between the hits: Total correlations between all traversals are calculated by replacing $P_D(L) \times T$ and $P_T(L) \times T$ in equation (1) by $\sum_{N_{hit}} \left(P_D(L) \times T\right)$ and $\sum_{N_{hit}} \left(P_T(L) \times T\right)$, which represent the total probabilities of hitting targets related to cell killing and cell inactivation, respectively, when N_{hit} traversals occur simultaneously in the cell nucleus.

RESULTS

In the present work, two characteristic exposure conditions were investigated: (i) a lifetime residential indoor exposure of 20 Working Level Months (WLM)[2], and, (ii) a cumulative exposure of 578.6 WLM over a 4 years working period, representing the average exposure measured in Colorado mines[3]. The source densities of alpha particle emissions were 3.28×10^4 (^{218}Po) and 3.85×10^4 (^{214}Po) alpha particles per cm^2 for residential chronic exposure, and 1.49×10^4 (^{218}Po) and 2.24×10^4 (^{214}Po) alpha particles per cm^2 for occupational uranium miner exposures, normalized to a cumulative exposure of 1 WLM[17,20]. Microdosimetric simulations were performed for spherical cell nuclei of 9 μm diameter, located at 20 μm (secretory cells) and 40 μm (basal cells) depth[30] in bronchial epithelium of airway generation 4 (for the cylindrical geometry) and airway generations 3-4 (for the bifurcation geometry), respectively, which are representative of the bronchial region where most bronchial carcinomas have been observed. The inhomogeneities of the radon progeny surface activities were identical to those already assumed for the microdosimetric calculations for bronchial cylindrical airways[16] and airway bifurcations[17].

Cylindrical airways

To evaluate the biological impact of non-uniform distributions of radon progeny surface activities in cylindrical airways, calculations were made for different source-target configurations characterizing the most relevant dosimetric scenarios[16]. Four illustrative cases were selected: A: uniform distribution of the activity, B: all the activity is concentrated in a hot spot of 10 × 10 μm and the target is situated at the same side of the cylinder (near wall), C: all the activity is again concentrated in a hot spot of 10 × 10 μm, but the target cell is situated at the opposite side of the

cylinder (far wall), and, D: all the activity is concentrated in a patch of 100 × 100 μm for the same conditions as in case B. The corresponding LET spectra, normalized to the number of hits, are presented in Figure 1 for target cells located at 20 μm (secretory cells) and 40 μm (basal cells) depths, assuming residential exposure conditions (related hit frequencies are listed in Table 1).

For the uniform distribution, LET spectra exhibit the same general features found in a previous study[20], varying within a wide range of values up to the maximum values of the two Bragg peaks. The peak around 100 keV μm^{-1} (related to maximum alpha energies) observed at 20 μm depth disappears at greater depths (40 μm), where the cells receive fewer hits (Table 1) but with higher energy transfers. For case B, cells located at 20 μm depth receive a number of hits higher which is about five orders of magnitude higher than those for the uniform distribution (Table 1), with two distinct LET peaks at about 80 keV μm^{-1} and 110 keV μm^{-1}, representative of the energies of the two alpha particles emitted from ^{214}Po and ^{218}Po. Because of the small size of the hot spot and the short distances to the target, the initial energy spectra are not yet appreciably distorted. At 40 μm, much fewer hits are recorded with LET values more widely distributed around peaks at 100 and 200 keV μm^{-1}. For target cells situated at the opposite side of the airway (case C, where the alpha particles have to cross the air volume and an additional mucus layer), the LET spectra still show distinct peaks, but with a wider dispersion at high LET values. When the source patch is extended to 100 × 100 μm (case D), the LET spectra are again widely distributed. Instead of the single peak at 100 keV μm^{-1} in panel A, two peaks can be observed at 80 and 120 keV μm^{-1}, representing the ^{214}Po and the ^{218}Po alpha particles, respectively. The significant variations of the LET spectra displayed in Figure 1 demonstrate that inhomogeneities

of the activity distribution and related source - target geometries can modify drastically the number of events, the LET distributions and, possibly, the resulting biological damage.

To assess the variability of the related biological effects, transformation probability spectra, normalized to the number of hits are plotted in Figure 2 for the same exposure conditions as for Figure 1 (average transformation probabilities are listed in Table 1), varying over a wide range of about five orders of magnitude (from 10^{-9} to 7.8×10^{-4}).

The shapes of the transformation probability spectra result from a complex combination of the track length and LET distributions and the way they affect cellular inactivation. For the uniform case (panel A), all transformation probabilities (except the very small values) have nearly the same relative frequency with a small and broad peak at about 4×10^{-4}. At 40 μm depth, the much fewer hits experienced by the cell possess a higher transformation potential, reflecting the higher LET values. The distinct peaks at small transformation probabilities (less than 2×10^{-5}) are due to alpha particles crossing the target with very small track lengths and energy values. In panel B, the transformation probabilities simply reflect the triangular chord length distributions of the two alpha particles. The dispersions and the relative magnitudes of the triangular distributions depend on the selected target diameter and the LET values at the peaks in panel B of Figure 1. While the triangular distributions are still discernible at 20 μm depth in panel C, the small number of hits of ^{218}Po alpha particles hardly contributes to the transformation probability at 40 μm depth. When the activity patch is 100 × 100 μm (case D), the spectra cover again the whole range of possible transformation probabilities, reflecting the corresponding LET distributions in Figure 1.

It is interesting to note that the transformation probabilities per surviving cell in single traversals never exceed a maximum value of about 7.8×10^{-4}. Analyses of the Monte Carlo results

reveal that the maximum values correspond to alpha particles crossing the target with nearly maximum chord length (from 8.7 to 9 μm) and with LET values in the range of 170 to 180 keV μm^{-1}. To illustrate the effect of LET and track length on the transformation potential of the alpha particles, transformation probabilities were calculated analytically for different track lengths as a function of LET, where the 6 μm and 9 μm track lengths represent average and maximum track lengths in the cell nucleus (Figure 3).

While the transformation probabilities increase almost linearly for small track lengths, their values reach a maximum at higher track lengths and then decrease because of the increasing efficiency of cell inactivation at high LET values. The maximum value of the transformation probability is 7.79×10^{-4} for a diameter of 9 μm and an LET equal to 175 keV μm^{-1}, which is in good agreement with the values obtained by the Monte Carlo code.

Hit frequencies and average transformation probabilities for single and multiple hits (correlated and uncorrelated) are presented in Table 1 for the same activity distributions exhibited in Figures 1 and 2. Calculations were made for basal and secretory cell nuclei during a cell turnover time of 30 days and a lifetime residential exposure of 20 WLM. For single traversals, average transformation probabilities at a given depth vary only slightly among the four activity patterns. While the lower transformation values in case B are caused by the lower LET values in this configuration, deeper lying basal cells have a higher probability to be transformed when traversed by a single alpha particle due to the higher LET values at this depth. In contrast to single traversals, multiple hit transformation probabilities vary by many orders of magnitude as a result of the related variations of the hit frequencies. In case of multiple hits, the higher oncogenic potential of basal cells for single hits is offset by the much higher particle fluence in secretory cells. Nevertheless, target cells receive multiple hits only in the few cases when they are

very close to the hot spot. Indeed, a detailed analysis of the hit probabilities around a cylindrical airway for non-uniform exposures revealed that hit probabilities rapidly decrease by many orders of magnitude for target cells distant from the source patch either in the direction of the central axis (along a distance of 80 μm) or around the radial angle[16]. Hence, transformation probabilities for correlated traversals are presented only for cases B and D. The results listed in Table 1 indicate that the most exposed cells are not necessarily the cells with the highest transformation frequencies, as the cells very close to the hot spot are most likely inactivated.

The effect of particle traversal correlations on the assessment of oncogenic transformations is illustrated in Figure 4 for alpha particles with LET values of 60 and 120 keV μm^{-1} by plotting the transformation probability as a function of the number of hits for both uncorrelated and totally correlated hits, assuming an average chord length of 6 μm. For non-correlated traversals, the transformation probability increases linearly with the number of hits with a rate depending on the single hit transformation potential for that LET value. Assuming a monoclonal origin of cancers[3], the assumption of independent hits is consistent with the linear non-threshold hypothesis. Below a given number of hits, the correlation produces higher transformation probabilities and thus higher carcinogenic risk relative to the linear relationship predicted for uncorrelated traversals. Above these limiting hit numbers, the hit correlations induce an inverse effect, due to cell inactivation that reduces the transformation potential relative to the linear assumption. The limiting numbers depend on LET and track length of the traversing alpha particles. For instance, they adopt values of 20, 10 and 3 for 40, 60 and 120 keV μm^{-1}, respectively, for an average track length of 6 μm, i.e. the higher the LET and the track length (not shown in Figure 4), the lower is the limiting number of hits. The gray areas between the two

curves in Figure 4 encompass the whole range of potential transformation probabilities affected by exposure rate, repair mechanisms and cellular inactivation.

Airway bifurcations

Since airway bifurcations are of particular interest in radon progeny lung dosimetry and lung carcinogenesis, the effects of the different exposure conditions and target cell locations on oncogenic transformations were investigated for an idealized symmetric bifurcation model[31]. As shown in Figure 5, the bifurcation is composed of three successive regions: (i) the cylindrical parent branch, (ii) the central Y-shaped bifurcation zone, and (iii) the two cylindrical daughter branches. The carinal ridge is the site where the two central zone branches are joined together. The linear dimensions of bifurcation geometry used in the present study correspond to airway generations 3-4 of Weibel´s lung model A[32]. The target cell nuclei are assumed to lie at different depths within the bronchial epithelial layer surrounding the whole bifurcation. Calculations of transformation probabilities were made for different target cell positions representing key locations in the bifurcation [17]: carinal ridge (T), parent branch-central zone connection (R_1), and central zone (R_2) (see Figure 5). The non-uniform distribution of the surface activity is represented by radon progeny accumulations at the carinal ridge covering 10% of the bifurcation area, which is equivalent to two patches of about 0.45×0.45 cm on each side of the carinal ridge[8]. The enhancement of the surface activity at the carinal ridge is quantified by a carinal ridge surface density ratio of 7, defined as the average surface density of deposition within the carinal ridge divided by the average surface density within the whole bifurcation, for both attached and unattached radon progeny[8].

The LET spectra for target cell nuclei located at 20 and 40 μm depth at the carinal ridge (T) and at the central zone (R_2) are plotted in figure 6 for both uniform and non-uniform surface activities, normalized to the number of hits related to uranium miner exposure conditions. The spectra are quite similar for all selected target locations, including location R_1 (not shown in Figure 6). However, one can note a higher frequency of high LET values relative to low LET values in the carinal zone as compared to location R_2 due to the longer distances traveled by the alpha particles. The LET spectra for the deeper lying basal cells (40 μm depth) indicate that these cells receive fewer hits than the secretory cells (20 μm depth), but with higher energy transfer. The similarity of the LET spectra for uniform and non-uniform activity distributions is due to the comparatively large surface areas of the patches relative to alpha particle ranges. LET spectra for residential radon exposures are the same as those shown in Figure 6 for uranium miners, except for their lower relative frequency.

Corresponding transformation probability spectra, normalized to the number of hits, for secretory and basal cell nuclei are displayed in Figure 7 for uranium miner exposure conditions (average transformation probabilities are listed in Tables 4 and 5). The shapes of the spectra are quite similar for both uniform and non-uniform activity distributions as well as for all selected target locations, including location R_1 (not shown in Figure 7). Since these spectra represent the interaction of the LET spectra with the triangular track length distributions, similar LET distributions (see Figure 6) lead to similar transformation probability distributions, while the relative frequencies reflect the number of related alpha particle hits (see Tables 4 and 5). Likewise, transformation probabilities for the basal cells are shifted to higher values because of the respective shifts in the LET spectra. Corresponding transformation probability spectra for residential radon exposures are the same as those shown in Figure 7 for uranium miners, except

for their lower relative frequency. The same analyses of the effects of LET and track length on transformation probabilities, as already illustrated in Figure 3 for cylindrical airways, also apply to the bifurcation geometry.

Related hit frequencies and average transformation probabilities for residential exposure conditions are listed in Tables 2 and 3 for secretory and basal cells. In case of a uniform distribution of the activity, hit frequencies are higher than those for the cylindrical geometry (Table 1) because of differences in geometry and source volumes. Single traversals of alpha particles at a given depth have approximately the same transformation potential at all target locations. However, transformation probabilities may decrease by some orders of magnitude if normalized to the hit frequency. Since target cells primarily receive single hits in residential exposures, even for highly localized alpha emitters in the carinal zone, only uncorrelated transformation probabilities are presented in Tables 2 and 3. While transformation probabilities for single traversals are higher for the basal cells than for the secretory cells, the uncorrelated transformation probabilities are smaller due to their lower number of hits.

In uranium miner exposure situations, miners are subject to higher exposures within relatively short periods of time and single cells receive a significantly higher number of hits. Related hit frequencies and average transformation probabilities for average Colorado mining conditions (578.6 WLM) during an average working period of 4 years[3] are presented in Tables 4 and 5 for secretory and basal cells. In case of a uniform activity distribution, individual cells still experience primarily single traversals, even for such high exposures. In contrast, localized activity distributions result in multiple traversals at the carinal ridge, inducing transformation probabilities which are up to two orders of magnitude higher than those in the rest of the bifurcation. Since only the target cells located at the carinal ridge receive an appreciable number

of multiple hits, correlated transformation probabilities are presented in Tables 4 and 5 for these cells. The carinal ridge remains the zone with the highest oncogenic potential, even if the nuclear traversals are assumed to be totally correlated, i.e. for the simultaneous traversals of the alpha particles associated with a higher inactivation probability. For the non-uniform activity distribution, uncorrelated transformation probabilities for basal cells at the carinal ridge are smaller than those for secretory cells because of the smaller number of hits. By the same token, however, correlated transformation probabilities exhibit the opposite behavior as fewer hits reduce the related cell killing efficiency.

To relate transformation probabilities in target cells to lung cancer incidence, transformation probabilities for secretory and basal cells located at the carinal ridge (T) are plotted in Figure 8 as functions of the cumulative exposure for uranium miner exposure conditions, illustrating the effects of correlated and uncorrelated nuclear traversals for uniform (panel A) and non-uniform (panel B) surface activity distributions. The conversion factors relating the number of hits to WLM depend on exposure condition, location of target cell and depth in epithelium and can be obtained from Tables 2 - 5. As already discussed in Figure 4, uncorrelated transformation probabilities produce a linear dose-effect relationship, the slope of which depends on the single hit transformation probability and the number of hits per WLM. For correlated transformation probabilities a consistent pattern can be observed. Transformation probabilities first increase in a sublinear fashion, then exceed the linear predictions, and subsequently bend over when exceeding a defined exposure level (or number of hits) due to the increasing efficiency of cell killing. While the maximum transformation probability remains practically unchanged, related exposure levels vary with activity distribution and cell type. Although the number of hits producing the maximum transformation probability are similar for

both cell types (2.61 vs. 2.48 for secretory cells and 2.19 vs. 2.28 for basal cells), the maximum for the non-uniform distribution is shifted to smaller exposure levels by about an order of magnitude. These differences in exposure level reflect corresponding differences in the number of hits (see Table 4), which are higher by about an order of magnitude for the non-uniform activity distribution, i.e. higher hit frequencies lead to a maximum at smaller exposure levels. Thus for a given cell depth, differences in activity distributions can simply be scaled by the hit frequency. In contrast, hit numbers related to the maximum transformation probability are consistently smaller for basal cells than for secretory cells (2.19 vs. 2.61 for the non-uniform distribution and 2.28 vs. 2.48 for the uniform distribution). These differences reflect the higher LET values in basal cells (see Figure 6) and the resulting shift of the maximum to lower hit numbers (see Figure 4). Thus the higher exposure levels associated with the maximum transformation probabilities for the basal cells by about a factor of 2 can again be explained by the smaller number of hits (see Table 4), although slightly modified by corresponding differences in the LET spectra.

DISCUSSION

Microdosimetric spectra and hit frequencies, computed for different airway geometries and surface activity distributions were interpreted in terms of oncogenic transformations to assess the biological effects of radon progeny alpha particles in the human respiratory tract. The oncogenic transformations were simulated for the exact numbers of hits received by cell nuclei at given exposure conditions. This is motivated by micro-beam experiments[25] which showed that (i) oncogenicity from exactly one hit was lower than the Poisson distributed mean of one alpha

hit, and (ii) cells traversed by multiple hits contribute more to the risk than the ones traversed by exactly one single particle. In the present study, the track structure of alpha particles was described by the LET, since the experimental in vitro transformation data utilized for the biological effect predictions were reported in terms of LET[23]. While average single hit transformation probabilities exhibit only slight variations, individual single hit transformation probabilities can vary by about five orders of magnitude, indicating that lung cancer risk assessments should be based on full distributions rather than on single average values.

The location of target cells relative to non-uniform surface activity distributions strongly affect the number of hits, LET distributions and related transformation probability spectra of basal and secretory cells. Average transformation probabilities are considerably enhanced for radon progeny accumulations and target cells at the carinal ridge, relative to uniform activity distributions and target cells located along curved and straight airway portions at the same exposure level. This supports the hypothesis, as surmised by particle deposition and histological studies, that target cells located at the carinal ridge may indeed play a key role in the development of bronchial carcinomas[12].

In the present study, energy deposition is simulated in single cells with a cycle time of 30 days, i.e. each epithelial cell at a given site is replaced by a new one after about 30 days, in agreement with the BEIR IV report [3,29]. However this value should be taken cautiously and additional studies may be needed for a more precise determination of cell cycle times for different epithelial cells, as cycle times may be different for basal and secretory cells. It is further assumed that any damage to this cell as a result of multiple hits is only accumulated over the lifetime of that cell, but does not affect the probability of cellular survival or transformation of the cell replacing the originally hit cell at that site. Thus hit frequencies in Tables 1 - 5 have to be

multiplied by the ratio of the exposure time divided by the cycle time of 30 days (e.g. by a factor of 48 in case of uranium miner exposures) to give the total number of hits at a given location during the full period of exposure.

Experimental transformation data for C3H 10T1/2 cells were applied for the predictions of transformation probabilities in bronchial target cells as transformation frequencies for different LET values are presently only available for this cell line to derive probabilities-per-unit-track-lengths for oncogenic transformation as a function of LET[20]. To extrapolate the findings presented in this paper to in vivo carcinogenesis in the human lung, differences between immortalized mouse embryo fibroblasts and primary epithelial lung cells must be considered.

Recent studies of in vitro transformation in rat tracheal epithelial (RTE) cells by alpha particles with an LET of 135 keV μm^{-1} [33] indicated that the shape of the dose-effect relationship up to about 1 Gy was practically the same as that for the mouse embryo fibroblast C3H 10T1/2 cells[23] for LET values of 120 and 150 keV μm^{-1}, although C3H 10T1/2 cell were about 15 times more sensitive that the RTE cells. This suggests that the shapes of our predicted transformation curves are not appreciably affected by cell type, differing only in the absolute numbers. Since no information is presently available on the LET dependence of the RTE cells, it is assumed to be the same as for the C3H 10 T1/2 cells. Likewise, the same radiosensitivity is assumed for secretory and basal cells, consistent with the current view of ICRP[34] that both cells contribute to bronchial dose with equal weight. Regarding the immortalization of the cell lines, which is a necessary requirement to perform experimental transformation studies, it is assumed that immortalization is unrelated to the steps leading to initiation and promotion. Instead, immortalization is interpreted to allow initiated and promoted cells to grow into preneoplastic

lesions, thus affecting only the absolute values of the transformation frequencies but not their dependence on dose and LET.

The subsequent comparison with epidemiological data is based on the assumption that lung cancer incidence is proportional to the transformation probability for a single cell with respect to the shape of the dose-effect relationship, but not to the absolute numbers. Epidemiological studies of lung cancer incidence in uranium miners indicate that (i) relative risk starts to deviate from linearity in a downwards fashion between 300 and 500 WLM[35], and (ii) a marked inverse dose rate effect was observed at exposures above 400 WLM[3]. Both observations are in good agreement with the predictions for non-uniform activities, displayed in Figure 8, panel B, where the intersection of uncorrelated and correlated transformation probabilities ranges from roughly 300 (secretory cells) to 600 WLM (basal cells). In contrast, corresponding exposure levels for the uniform activity distribution would lead to unrealistically high exposure levels, ranging from about 4000 (secretory cells) to 7000 WLM (basal cells), i.e. about an order of magnitude higher. This suggests that the inhomogeneity of radon progeny surface activities must be considered in lung cancer risk assessment. In further consequence, the higher doses received by the target cells located at the carinal ridge imply a larger dose-exposure conversion factor than currently assumed on the basis of uniform surface activities[5, 7]. Although a larger dose-exposure conversion factor would further increase the still existing discrepancy between the conversion factors based on dosimetry and epidemiology, it may be compensated by a smaller radiation weighting factor[21].

The similarity of the shapes of the dose-effect curves for transformation probabilities and lung cancer incidence further indicates that correlated transformation probabilities must be considered for uranium miner exposures, which is consistent with the view that dose rate is a

more appropriate indicator of risk than dose. The observation that correlated transformation probabilities due to multiple hits are occurring nearly exclusively at carinal ridges further corroborates histological findings that bronchial tumors are primarily induced within bronchial airway bifurcations.

Despite the apparent similarity of the shapes of the dose-effect curves for transformation probabilities and lung cancer incidence, it must be pointed that many factors not considered in the above comparison may eventually modify the predicted dose-effect curves. This includes experimentally observed cellular effects at the local and temporal scale, such as the bystander effect, adaptive response or genomic instability, the in vivo response of cells in an interacting tissue volume as compared to in vitro conditions, and the promotional role of radiation or other inhaled substances. Furthermore, the initiation phase may be protracted over the assumed period of pulmonary epithelium renewal, leading to a delayed neoplastic development. The effects of such factors are currently investigated by incorporating microdosimetric and multiple hit considerations into a biologically-based state vector model of carcinogenesis[36]. While caution must be exercised in applying the above conclusions to the estimation of lung cancer risk in humans, the present simulations may still be able to predict trends relevant to radon-induced lung cancer risk.

To compare our predictions to epidemiological data on lung cancer incidence, one must bear in mind that cigarette smoking is the largest confounder, particularly for uranium miners, where the vast majority of bronchial carcinomas was found in smokers[35]. While our present simulations are based on the normal lung morphology, physiology, and histology of a healthy non-smoker, significant effects of cigarette smoking on these factors have been reported, such as airway narrowing, higher breathing frequency, increased mucus production, reduced mucociliary

clearance, increased thickness of the bronchial epithelium, and changes in epithelial cell population[34]. Recent dose calculations indicated that resulting cellular doses range from slightly smaller values in short-term smokers to moderately higher doses in long-term smokers, with a maximum enhancement factor of 1.6. In terms of microdosimetry, the higher cellular doses in long-term smokers are related to larger number of cellular hits and higher LET values, which may lead to slightly higher transformation frequencies. Thus we do not anticipate that cigarette smoking will appreciably affect the shapes the transformation functions predicted for non-smokers. The additional carcinogenic effect of smoking will, however, increase the absolute magnitude of lung cancer risk in a multiplicative fashion[3].

The primary objective of the present study was to relate the microdosimetric spectra resulting from the inhomogeneity of radon progeny surface activities in bronchial cylindrical airways[16] and airway bifurcations[17] to resulting biological effects in bronchial epithelial cells of biological relevance. Thus transformation probabilities were calculated for selected representative locations of basal and secretory cells in bronchial airway generation 4 assuming different idealized source-target configurations. To extend the present microdosimetric simulations for selected cells and surface activity patterns to the whole bronchial tree, the range of basal and secretory cell depths in bronchial epithelium[34] in all bronchial airway generations must be factored into the analysis. Hence the comparison between the assumption of uniform activity distributions in infinitely long cylindrical airways, as is current practice in lung dosimetry, to realistic activity distributions in bronchial airway bifurcations will be the next step.

With respect to lung cancer risk at low doses, three conclusions may be drawn from the present study: (1) Since multiple hits hardly occur during the lifetime of an individual cell at low exposure levels, a linear dose response may be expected for low mining exposures (less then 200

WLM) and for long-term residential exposures. (2) Lung cancer incidence for short-term uranium miner exposures increases at intermediate exposure levels due to the correlation of multiple hits but decreases for higher exposures because of cell killing. (3) Since the frequency of multiple hits depends on dose rate, dose rate may be the primary reason for the deviation from the linear relationship and a major factor for any risk assessment based on multiple hit models.

The crucial question then is whether local inhomogeneities of radon progeny surface activities are more carcincogenic than uniformly distributed activities for the same total activity. A similar question was raised a few decades ago, where it was contended that lung deposition of alpha-emitting hot particles, especially plutonium and mixed transuranics, represent a lung cancer risk substantially greater than if the same amount of radionuclides were distributed rather uniformly[37]. While the available experimental data, comprising human and animal inhalation studies as well as in vitro transformation experiments provide controversial evidence[37,38], Charles et al.[38]recently concluded that the limited epidemiological data on lung cancer mortality following occupational inhalation of plutonium aerosols, and the incidence of liver cancer and leukemia due to thorotrast injection do not appear to support a significant enhancement factor, although a moderate enhancement factor cannot be ruled out[38,39].

Since no pertinent information about radon-induced lung cancer risk in bronchial airways is presently available, the following theoretical considerations may provide additional supporting evidence.

(i) A theoretical study of the carcinogenic risk of a hot particle composed entirely of the beta emitting ^{103}Ru indicated that cancer risk for this hot particle is higher than that for a uniform activity distribution only at intermediate activity levels, but smaller at high activities[40]. Since the

radon progeny hot spots at the carinal ridge are far below the activities measured for hot particles, a similar carcinogenic risk enhancement may also exist for radon inhalation.

(ii) The dose inhomogeneity in bronchial target cells is caused by the spatial correlation between the non-uniform activity distribution and the complex bifurcation geometry. In contrast, the epidemiological data for plutonium and transuranium nuclide inhalation[37] refer to the dose distribution in the alveolar region of the lung, which has a rather uniform target geometry and thus would not a show a similar spatial correlation. In addition, the activities of the radon progeny hot spots are orders of magnitude smaller than those for the plutonium hot particles.

(iii) A peculiar feature of radiation-induced carcinogenesis in German thorotrast patients is that no excess lung cancers have been observed so far in the epidemiological follow-up studies, although application of the current risk coefficient derived from the inhalation of radon progeny would predict an observable excess of lung cancer cases. In contrast to the enhanced radon progeny deposits at carinal ridges during inspiration, most of the exhaled thoron progeny decay while transported in the exhaled airstream, thus producing a rather uniform dose distribution in epithelial target cells[41]. This difference in dose distribution may be one of the explanations why bronchial carcinomas have been observed in radon inhalation but not in thoron exhalation as in thorotrast patients.

(iv) Histological studies have revealed that neoplastic and preneoplastic lesions are preferentially observed at carinal ridges[14,15]. Although most of them may have been induced by cigarette smoke, the main cause of lung cancer, deposition and resulting accumulation patterns of cigarette smoke particles within bronchial airway bifurcations are practically the same as those for radon progeny. Hence, neoplastic and preneoplastic lesion induced by radon progeny alpha

particles may also occur primarily at carinal ridges, consistent with the predicted microscopic dose distributions.

The above considerations seem to explain the limited applicability of some negative epidemiological results and/or support the existence of a carcinogenic enhancement effect for radon progeny accumulations in bronchial airway bifurcations. However, consistent with the conclusions of Charles et al.[37], we do not expect enhancement factors as high as a few orders of magnitude as originally claimed at the peak of the hot particle controversy[43], but rather a more moderate effect.

ACKNOWLEDGEMENTS

This research was supported in part by the Commission of the European Communities under Contract FI6R-CT-2003-508842. The authors also gratefully acknowledge the support of Pascal Pihet and the contribution of David E. Charlton in the initial development of the microdosimetric code.

REFERENCES

1. Caswell R. S., Coyne J. J. Microdosimetry of radon and radon daughters. Radiat. Prot. Dosim. **31**, 395-398 (1990).

2. National Research Council (NRC). Comparative dosimetry of radon in mines and homes. Washington DC: National Academy Press (1991).

3. National Research Council (NRC). Health effects of exposure to radon (BEIR VI). Washington DC: National Academy Press (1999).

4. Zock C., Porstendörfer A., Reineking A. The influence of biological and aerosol parameters of inhaled short-lived radon decay products on human lung dose. Radiat. Prot. Dosim. **63**, 197-206 (1996).

5. Marsh J. W., Birchall A. Sensitivity analysis of the weighted equivalent lung dose per unit exposure from radon progeny. Radiat. Prot. Dosim. **87**, 167-178 (2000).

6. Nikezic D., Yu K. N. Distributions of specific energy in sensitive layers of the human respiratory tract. Radiat. Res. **157**, 92-98 (2002).

7. Winkler-Heil R., Hofmann W. Comparison of modeling concepts for radon progeny lung dosimetry. In: Burkart W., Sohrabi M., Bayer A., editors. High levels of natural radiation and radon areas: Radiation dose and health effects. Amsterdam: Elsevier. 169-177 (2002).

8. Hofmann W., Martonen T. B., Ménache M. G. A dosimetric model for localised radon progeny accumulations at tracheobronchial bifurcations. Radiat. Prot. Dosim. **30**, 245-259 (1990).

9. Martonen T. B., Hofmann W. Dosimetry of localised accumulations of cigarette smoke and radon progeny at bifurcations. Radiat. Prot. Dosim. **38**, 81-89 (1991).

10. Kinsara A. A., Loyolka S. K., Thompson R. V., Miller W. H., Holub R. F. Deposition patterns of molecular phase radon progeny (^{218}Po) in lung bifurcations. Health Phys. **68**, 371-382 (1995).

11. Balásházy I., Hofmann W. Quantification of local deposition patterns of inhaled radon decay products in human bronchial airway bifurcations. Health Phys. **78**,147-158 (2000).

12. Balásházy I., Hofmann W., Heistracher T. Local particle deposition patterns may play a key role in the development of lung cancer. J. Appl. Physiol. **94**, 1719-1725 (2003).

13. Balásházy I., Farkas A., Szöke I., Hofmann W., Sturm R. Simulation of deposition and clearance of inhaled particles in central human airways. Radiat. Prot. Dosim. **105**, 129-132 (2003).

14. Garland L. H. Bronchial carcinoma. Lobar distribution of lesions in 250 cases. Calif. Med. **94**, 7-8 (1961).

15. Garland L. H., Beier R. L., Coulson W., Heald J. H., Stein R. L. The apparent sites of origin of carcinomas of the lung. Radiology **78**, 1-11 (1962).

16. Fakir H., Hofmann W., Caswell R. S., Aubineau-Laniece I. Microdosimetry of inhomogeneous radon progeny distributions in bronchial airways. Radiat. Prot. Dosim. **113**, 129-139 (2005).

17. Fakir H., Hofmann W., Aubineau-Laniece I. Microdosimetry of radon progeny alpha particles in bronchial airway bifurcations. Radiat. Prot. Dosim. 10.1093/rpd/nci314.

18. Crawford-Brown D. J., Hofmann W. An effect-specific track length model for radiations of intermediate to high LET. Radiat. Res. **126**, 162-170 (1991).

19. Crawford-Brown D. J., Hofmann W. Correlated hit probability and cell transformation in an effect-specific track length model applied to in vitro alpha irradiation. Radiat. Environ. Biophys. **40**, 317-323 (2001).

20. Hofmann W., Ménache M. G., Crawford-Brown D. J., Caswell R. S., Karam L. R. Modeling energy deposition and cellular radiation effects in human bronchial epithelium by radon progeny alpha particles. Health Phys. **78**, 377-393 (2000).

21. Hofmann W., Fakir H., Aubineau-Laniece I., Pihet P. Interaction of alpha particles at the cellular level - implications for the radiation weighting factor. Radiat. Prot. Dosim. **112**, 493-500 (2004).

22. International Commission on Radiation Units and Measurements (ICRU). Microdosimetry. ICRU Report 36. Washington DC: ICRU (1983).

23. Miller R. C., Marino S. A., Brenner D. J., Martin S. G., Richards M., Randers-Perhson G., Hall E. J. The biological effectiveness of radon progeny alpha particles. II: Oncogenic transformation as a function of linear energy transfer. Radiat. Res. **142**, 54-60 (1995).

24. Hofmann W., Crawford-Brown D. J., Fakir H., Caswell R. S. Energy deposition, cellular radiation effects and lung cancer risk by radon progeny alpha particles. Radiat. Prot. Dosim. **99**, 453-456 (2002).

25. Miller R. C., Randers-Pehrson G., Geard C. R., Hall E. J., Brenner D. J. The oncogenic transforming potential of the passage of single α particles through mammalian cell nuclei. Proc. Natl. Acad. Sci. USA **96**, 19-22 (1999).

26. Fakir H., Hofmann W., Aubineau-Laniece I., Caswell R. S., Jourdain J. R., Sabir A. Lung cancer risk in humans and rats: single vs. multiple exposures. In: McLaughlin J. P., Simopoulos S. E., Steinhäusler F., editors. The Natural Radiation Environment VII. Oxford: Elsevier. 1108-1115 (2005).

27. Leenhouts H. P., Chadwick K. H. A two-mutation model of radiation carcinogenesis: application to lung tumors in rodents and implications for risk evaluation. J. Radiol. Prot. **14**, 115-130 (1994).

28. Chadwick K. H., Leenhouts H. P., Brugmans M. J. P. A contribution to the linear no-threshold discussion. J Radiol Prot. **23**, 53-77 (2003).

29. Adamson I. Y. R. Cellular kinetics of the lung. In: Witschi H. P., Brian J. P., editors. Toxicology of inhaled materials. Berlin: Springer, 289-317 (1985).

30. Mercer R. R., Russell M. L., Crapo J. D. Radon dosimetry based on the depth distribution of nuclei in human and rat lungs. Health Phys. **61**, 117-130 (1991).

31. Heistracher T., Hofmann W. Physiologically realistic models of bronchial airway bifurcations. J. Aerosol Sci. **26**, 497-509 (1995).

32. Weibel E. R. Morphometry of the human lung. Berlin: Springer (1963).

33. Kugel C., Tourdes F., Poncy J. L., Fritsch P. RBE of α-irradiation for in vitro relative transformation of rat tracheal epithelial cells. Ann. Occup. Hyg. **46** (Suppl. 1), 285-287 (2002).

34. International Commission on Radiological Protection (ICRP). Human respiratory tract model for radiological protection. ICRP Publication 66, Ann. ICRP 24, Nos 1-3 (1994).

35. National Cancer Institute (NCI). Radon and lung cancer risk: a joint analysis of 11 underground miner studies. NIH Publication No. 94-3644. Bethesda, MD: National Cancer Institute (1994).

36. Fakir H., Hofmann W. Incorporation of microdosimetric concepts into a biologically-based model of radiation carcinogenesis. Radiat. Prot. Dosim. (Submitted [proceedings of 14th symposium on microdosimetry, Venice, 2005]).

37. International Commission on Radiological Protection (ICRP). Biological effects of inhaled radionuclides. ICRP Publication 31, Ann. ICRP 4, No 1/2 (1980).

38. Charles M. W., Mill A. J., Darley P. J. Carcinogenic risk of hot-particle exposure. J. Radiol. Prot. **23**, 5-28 (2003).

39. Mill A. J., Darley P. J., Charles M. W. Stochastic risks from 'hot particle' skin exposures. Radiat. Prot. Dosim. **92**, 151-160 (2000).

40. Hofmann W., Crawford-Brown D.J., Martonen T.B. The radiological significance of beta-emitting hot particles released from the Chernobyl nuclear power plant. Radiat.Prot. Dosim. **22**, 149-157 (1988).

41. Hofmann W., Hornik S. Lung dosimetry for Thorotrast patients: Implications for inhalation of radon progeny. Radiat. Res. **152**, S93-S96 (1999).

42. Tamplin A.R., Cochran T.B. Radiation standards for hot particles. Washington, DC: Natural Resources Defense Council (1974).

FIGURE CAPTIONS

Figure 1:

LET spectra of alpha particles in secretory (20 μm) and basal (40 μm) cell nuclei in bronchial epithelium of airway generation 4. The spectra are normalized to the number of hits due to the combined activity of ^{218}Po and ^{214}Po for a residential exposure of 1 WLM. A: uniform distribution of the activity, B: all the activity is concentrated in a hot spot of 10 × 10 μm and the target is situated at the same side of the cylinder (near wall), C: all the activity is again concentrated in a hot spot of 10 × 10 μm, but the target cell is situated at the opposite side of the cylinder (far wall), D: all the activity is concentrated in a patch of 100 × 100 μm for the same conditions as in case B.

Figure 2:

Single hit spectra of transformation probabilities in secretory (20 μm) and basal (40 μm) cell nuclei in bronchial epithelium of airway generation 4 for the same exposure conditions as in Figure 1.

Figure 3:

Transformation probabilities as functions of LET for different track lengths through a spherical cell nucleus with a diameter of 9 μm (average chord length = 6 μm).

Figure 4:

Transformation probabilities as functions of the number of hits for two LET values, 60 and 120 keV/µm, and an average chord length of 6 µm, comparing the effects of correlated and uncorrelated nuclear traversals. The areas between the two curves represent the potential variations of the transformation probability depending on dose rate, repair mechanisms and cellular inactivation.

Figure 5:

Schematic representation of the physiologically realistic bifurcation in the symmetry plane: P, parent branch; CA and CB, central zone branches; DA and DB, daughter branches. The considered target cells are located at different depths at T (carinal ridge), R_1 (parent branch-central zone connection) and R_2 (central zone).

Figure 6:

LET spectra of alpha particles in secretory (20 µm depth) and basal (40 µm depth) cell nuclei in the carinal ridge (T) and the central zone (R_2) of a symmetric airway generation 3-4 bifurcation. The spectra are normalized to the number of hits in a target cell nucleus due to the combined activity of ^{218}Po and ^{214}Po and an average cumulative exposure of uranium miners.

Figure 7:

Transformation probability spectra of alpha particles in secretory (20 μm depth) and basal (40 μm depth) cell nuclei in the carinal ridge (T) and the central zone (R_2) of a symmetric airway generation 3-4 bifurcation. The spectra are normalized to the number of hits in a target cell nucleus due to the combined activity of ^{218}Po and ^{214}Po and an average cumulative exposure of uranium miners.

Figure 8:

Transformation probabilities as functions of the cumulative exposure for secretory (20 μm depth) and basal cells (40 μm depth) located at the carinal ridge (T) of a symmetric airway generation 3-4 bifurcation for uranium miner exposure conditions, comparing the effects of correlated and uncorrelated nuclear traversals. The numbers on top of the uncorrelated transformation curves represent the hit frequencies corresponding to the maximum transformation probabilities.

Table 1:

Number of hits (N_{hit}), transformation probabilities for single hits (TF_{single}) and for multiple uncorrelated (TF_{unc}) and totally correlated (TF_{corr}) hits, at 20 μm (secretory cells) and 40 μm (basal cells) depth in bronchial epithelium of airway generation 4. Number of hits and transformation probabilities refer to individual cells with a cycle time of 30 days and a residential lifetime exposure (70 years) of 20 WLM. Panels A, B, C and D represent the four cases of activity distributions and irradiation geometry in cylindrical airways displayed in Figure 1.

	A		B		C		D	
	20 μm	40 μm	20 μm	40 μm	20 μm	40 μm	20 μm	40 μm
N_{hit}	4.13×10^{-4}	1.44×10^{-4}	39.77	5.7	5.36×10^{-4}	1.4×10^{-4}	6.95	1.35
TF_{single}	3.79×10^{-4}	4.28×10^{-4}	2.26×10^{-4}	4.07×10^{-4}	3.86×10^{-4}	4.96×10^{-4}	3.53×10^{-4}	3.88×10^{-4}
TF_{unc}	1.56×10^{-7}	6.16×10^{-8}	8.98×10^{-3}	2.32×10^{-3}	2.07×10^{-7}	6.97×10^{-8}	2.45×10^{-3}	5.24×10^{-4}
TF_{corr}	--	--	0*	1.9×10^{-4}	--	--	2.0×10^{-4}	5.8×10^{-4}

*Due to the high number of hits, the correlated transformation probability is extremely small that no value is given.

Table 2:

Number of hits (N_{hit}), transformation probabilities for single hits (TF_{single}) and for multiple uncorrelated (TF_{unc}) hits, for secretory cell nuclei at 20 μm depth in locations T, R_1 and R_2 of a symmetric bifurcation, representing the airway generation 3-4 juncture, for uniform and non-uniform source distributions. In case of the non-uniform distribution, local radon progeny accumulations are concentrated in two patches of size 0.45×0.45 cm around the carinal ridge. Number of hits and transformation probabilities refer to individual cells with a cycle time of 30 days and a residential lifetime exposure (70 years) of 20 WLM.

	T		R_1		R_2	
	Uniform	Non-uniform	Uniform	Non-uniform	Uniform	Non-uniform
N_{hit}	1.53×10^{-3}	1.86×10^{-2}	8.49×10^{-4}	7.15×10^{-5}	9.63×10^{-4}	6.51×10^{-4}
TF_{single}	3.8×10^{-4}	3.61×10^{-4}	3.79×10^{-4}	3.80×10^{-4}	3.92×10^{-4}	3.78×10^{-4}
TF_{unc}	5.85×10^{-7}	6.72×10^{-6}	3.22×10^{-7}	2.72×10^{-8}	3.78×10^{-7}	2.46×10^{-7}

Table 3:

Number of hits (N_{hit}), transformation probabilities for single hits (TF_{single}) and for multiple uncorrelated (TF_{unc}) hits, for basal cell nuclei at 40 μm depth in locations T, R_1 and R_2 of a symmetric bifurcation, representing the airway generation 3-4 juncture, for uniform and non-uniform source distributions. Source-target geometries and exposure conditions are the same as for Table 2.

	T		R_1		R_2	
	Uniform	Non-uniform	Uniform	Non-uniform	Uniform	Non-uniform
N_{hit}	5.96×10^{-4}	7.6×10^{-3}	3.05×10^{-4}	2.56×10^{-5}	3.46×10^{-4}	1.46×10^{-4}
TF_{single}	4.32×10^{-4}	4.3×10^{-4}	4.37×10^{-4}	4.38×10^{-4}	4.18×10^{-4}	3.07×10^{-4}
TF_{unc}	2.57×10^{-7}	3.27×10^{-6}	1.33×10^{-7}	1.12×10^{-8}	1.45×10^{-7}	4.48×10^{-8}

Table 4:

Number of hits (N_{hit}), transformation probabilities for single hits (TF_{single}) and for multiple uncorrelated (TF_{unc}) and correlated (TF_{corr}) hits, for secretory cell nuclei at 20 μm depth in locations T, R_1 and R_2 of a symmetric bifurcation, representing the airway generation 3-4 juncture, for uniform and non-uniform source distributions. Number of hits and transformation probabilities refer to individual cells with a cycle time of 30 days and an occupational exposure of 578.6 WLM during 4 working years to radon progeny in uranium mines. Source-target geometries are the same as for Table 2.

	T		R_1		R_2	
	Uniform	Non-uniform	Uniform	Non-uniform	Uniform	Non-uniform
N_{hit}	0.42	5.04	0.23	0.02	0.26	0.18
TF_{single}	3.78×10^{-4}	3.57×10^{-4}	3.76×10^{-4}	3.76×10^{-4}	3.92×10^{-4}	3.82×10^{-4}
TF_{unc}	1.60×10^{-4}	1.8×10^{-3}	8.77×10^{-5}	7.54×10^{-6}	1.03×10^{-4}	6.88×10^{-5}
TF_{corr}	--	4.83×10^{-4}	--	--	--	--

Table 5:

Number of hits (N_{hit}), transformation probabilities for single hits (TF_{single}) and for multiple uncorrelated (TF_{unc}) and correlated (TF_{corr}) hits, for basal cell nuclei at 40 μm depth in locations T, R_1 and R_2 of a symmetric bifurcation, representing the airway generation 3-4 juncture, for uniform and non-uniform source distributions. Source-target geometries and exposure conditions are the same as for Table 4.

	T		R_1		R_2	
	Uniform	Non-uniform	Uniform	Non-uniform	Uniform	Non-uniform
N_{hit}	0.17	2.12	0.085	0.0076	0.097	0.042
TF_{single}	4.32×10^{-4}	4.30×10^{-4}	4.37×10^{-4}	4.38×10^{-4}	4.18×10^{-4}	3.07×10^{-4}
TF_{unc}	7.34×10^{-5}	9.10×10^{-4}	3.73×10^{-5}	3.33×10^{-6}	4.07×10^{-5}	1.29×10^{-5}
TF_{corr}	--	8.40×10^{-4}	--	--	--	--

Figure 1

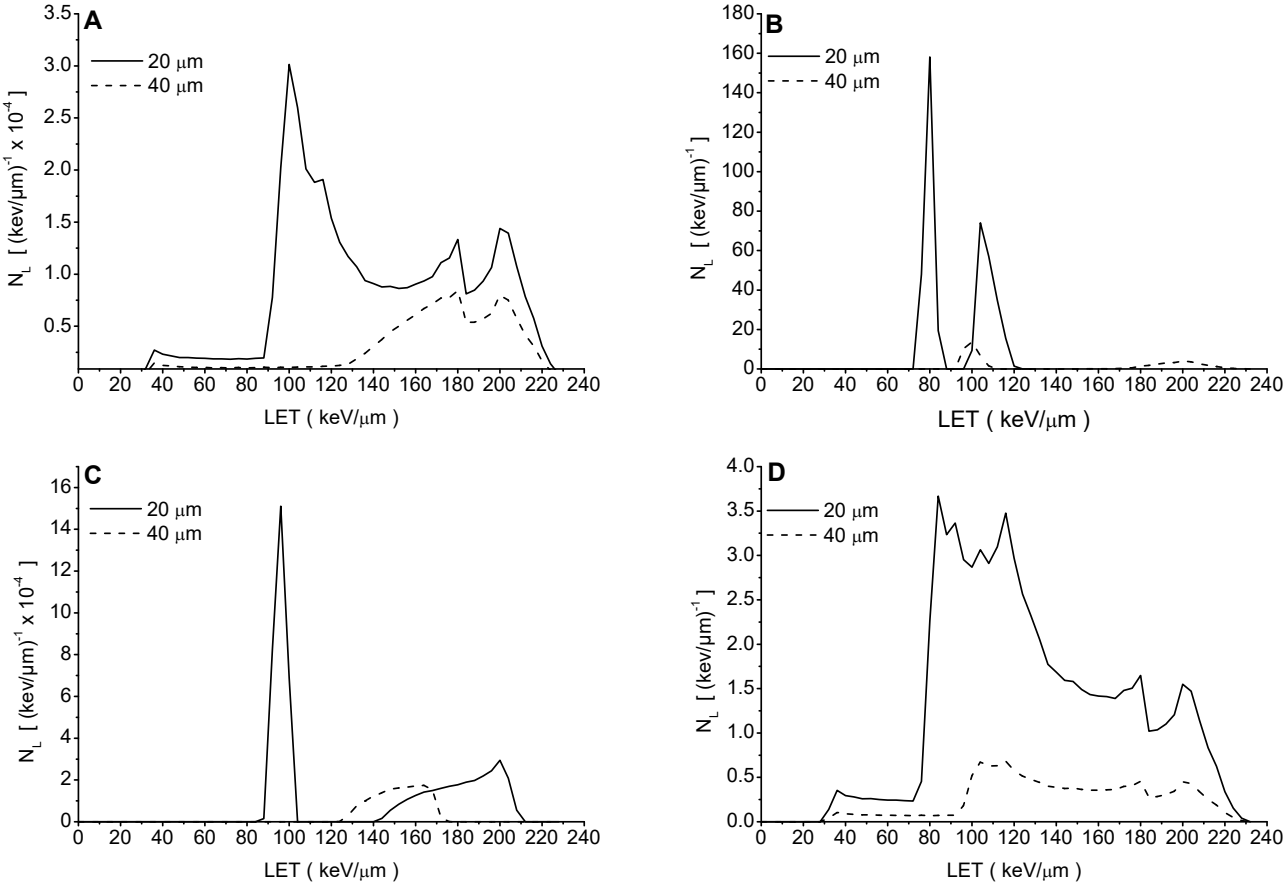
A
20 μm
40 μm
N_L [(kev/μm)^-1 x 10^-4]
LET (keV/μm)
B
20 μm
40 μm
N_L [(kev/μm)^-1]
LET (keV/μm)
C
20 μm
40 μm
N_L [(kev/μm)^-1 x 10^-4]
LET (keV/μm)
D
20 μm
40 μm
N_L [(kev/μm)^-1]
LET (keV/μm)

Figure 2

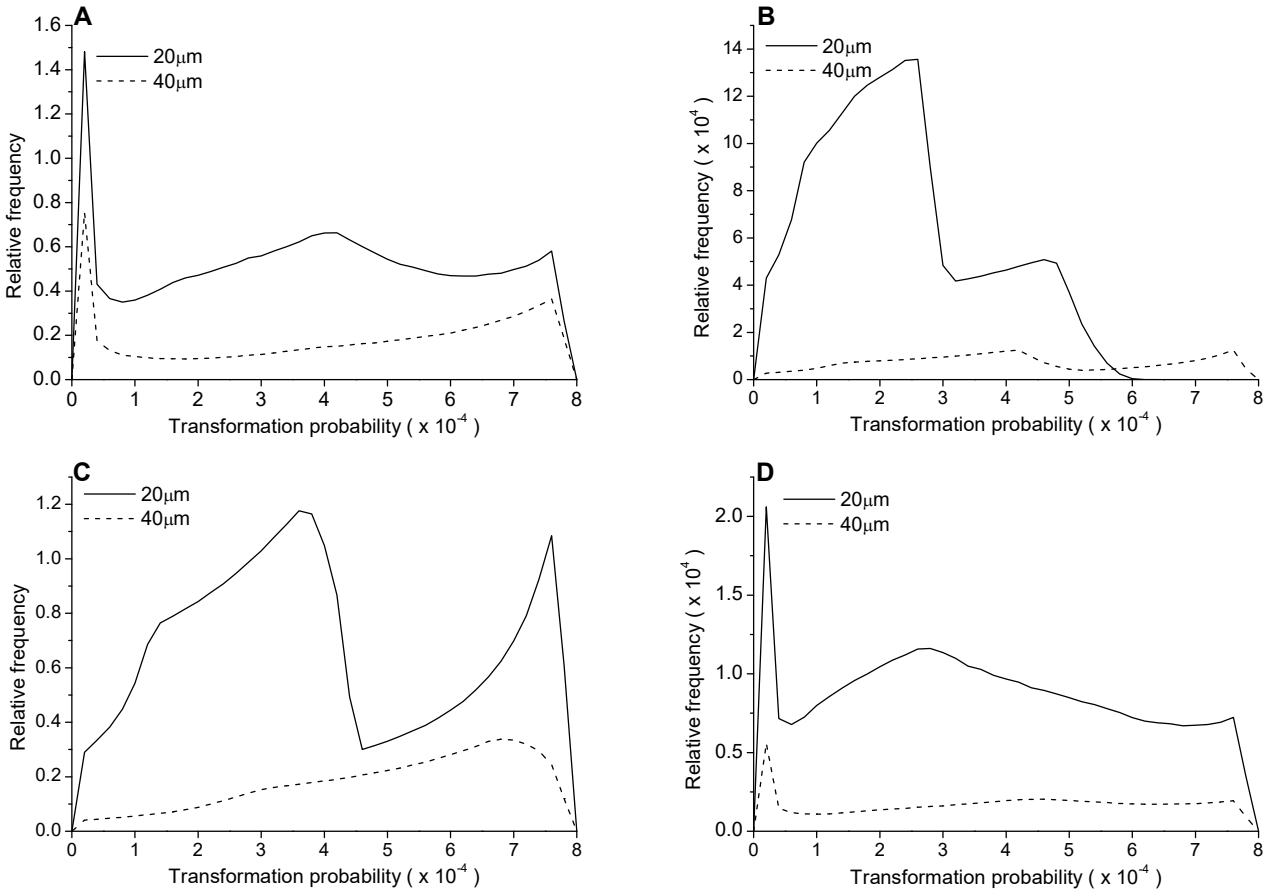
A
20μm
40μm
Relative frequency
Transformation probability (x 10-4)
B
20μm
40μm
Relative frequency (x 10-4)
Transformation probability (x 10-4)
C
20μm
40μm
Relative frequency
Transformation probability (x 10-4)
D
20μm
40μm
Relative frequency (x 10-4)
Transformation probability (x 10-4)

Figure 3

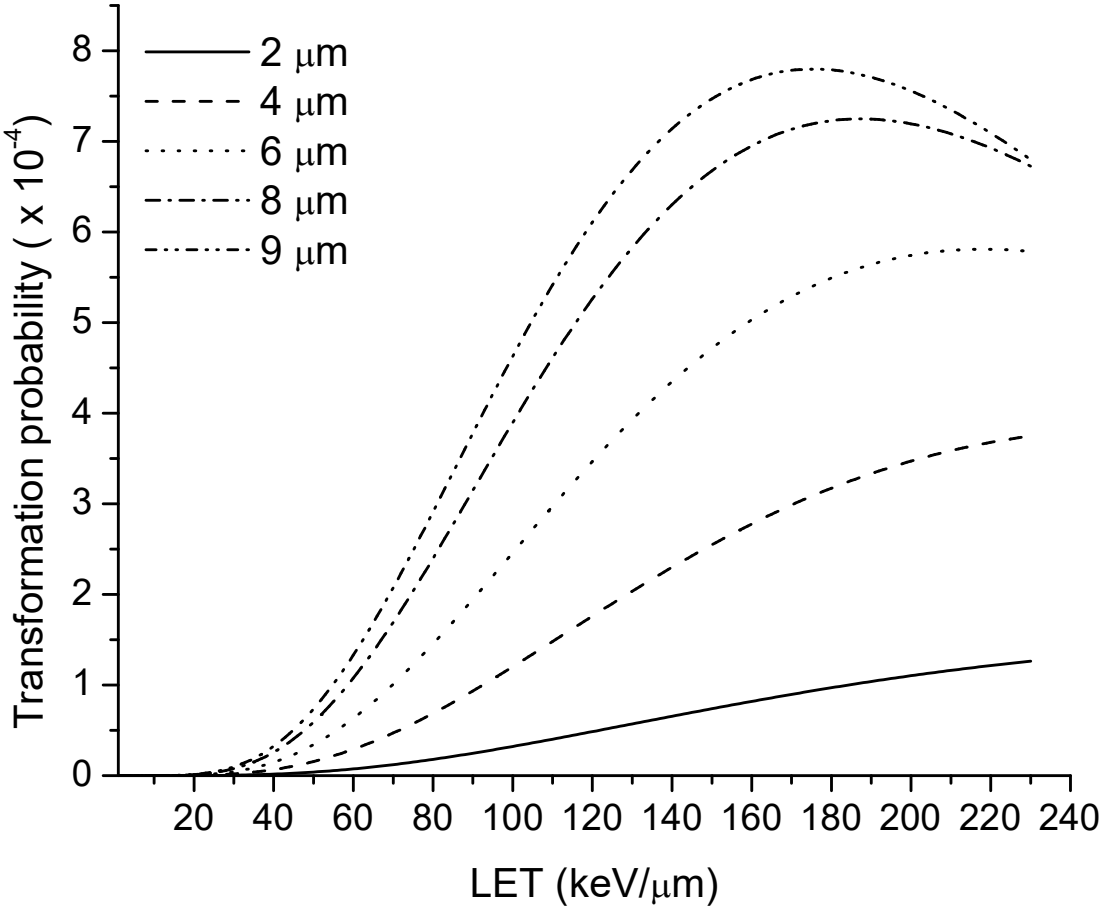
2 μm
4 μm
6 μm
8 μm
9 μm
Transformation probability (x 10^{-4})
0
1
2
3
4
5
6
7
8
20
40
60
80
100
120
140
160
180
200
220
240
LET (keV/μm)

Figure 4

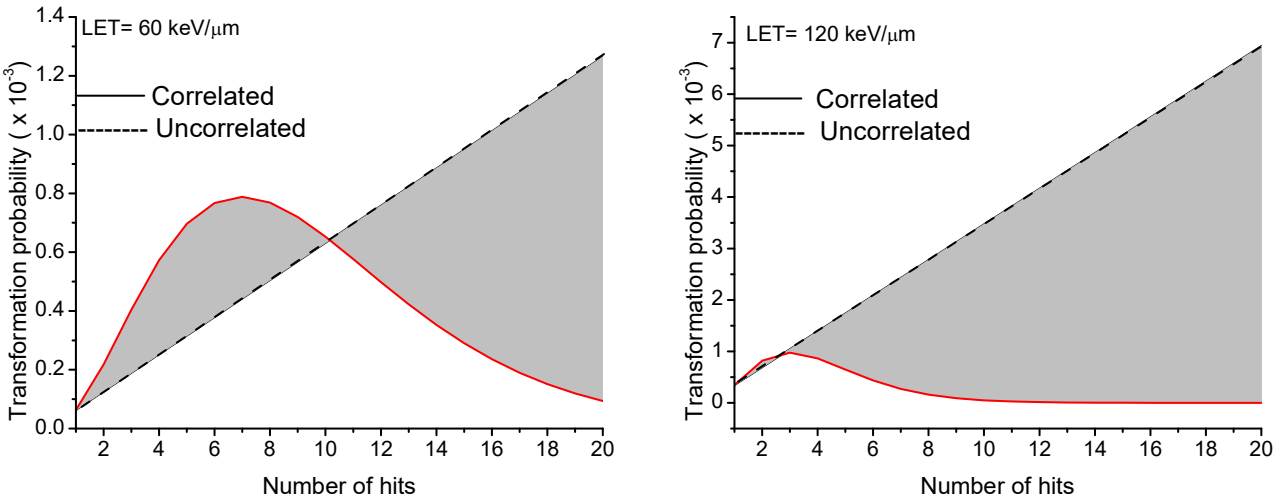
LET= 60 keV/μm
Correlated
Uncorrelated
Transformation probability (x 10^-3)
Number of hits
LET= 120 keV/μm
Correlated
Uncorrelated
Transformation probability (x 10^-3)
Number of hits

Figure 5

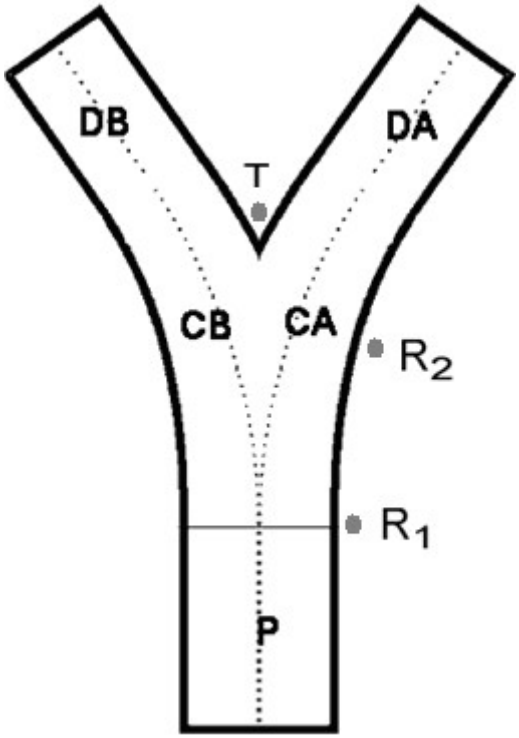

Figure 6

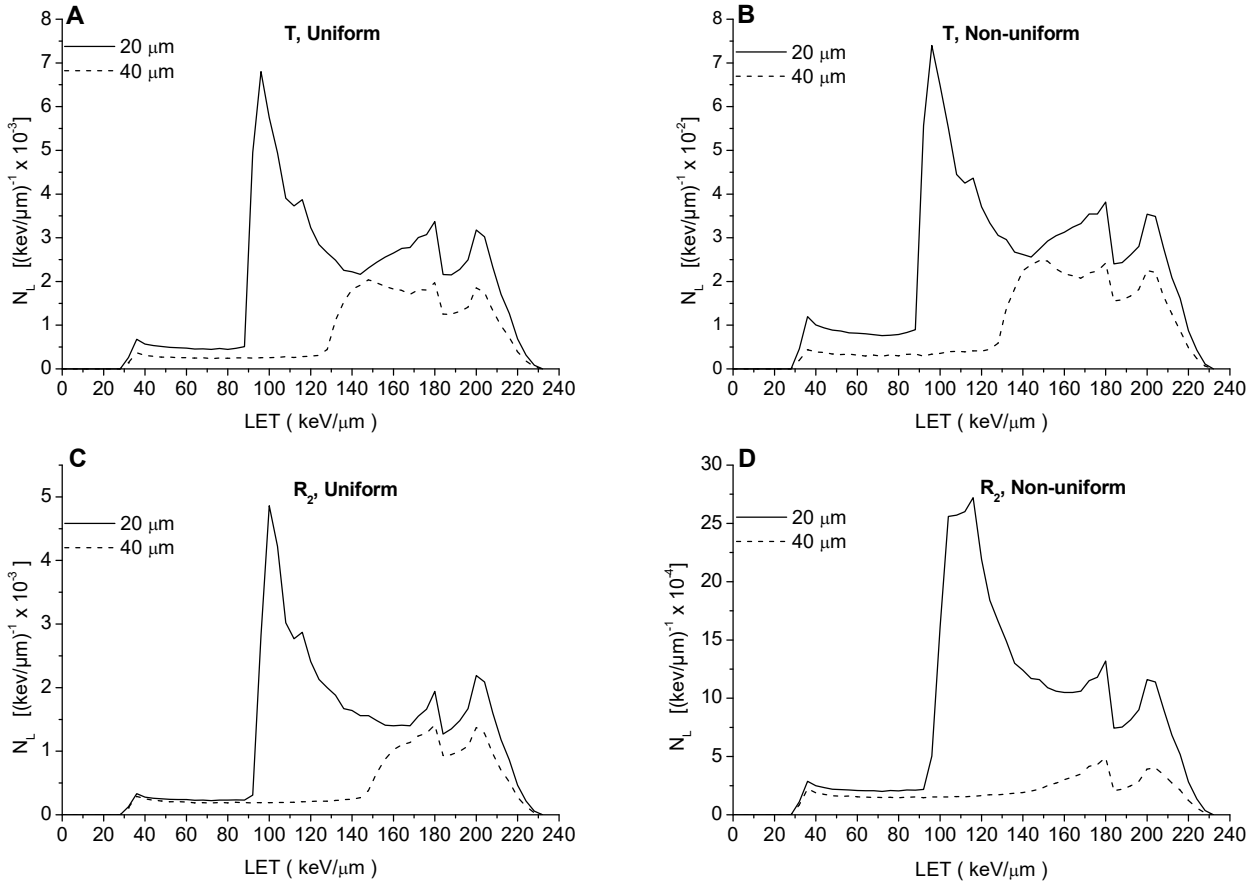
A
T, Uniform
20 μm
40 μm
N_L [(kev/μm)^-1 x 10^-3]
LET (keV/μm)
B
T, Non-uniform
20 μm
40 μm
N_L [(kev/μm)^-1 x 10^-2]
LET (keV/μm)
C
R2, Uniform
20 μm
40 μm
N_L [(kev/μm)^-1 x 10^-3]
LET (keV/μm)
D
R2, Non-uniform
20 μm
40 μm
N_L [(kev/μm)^-1 x 10^-4]
LET (keV/μm)

Figure 7

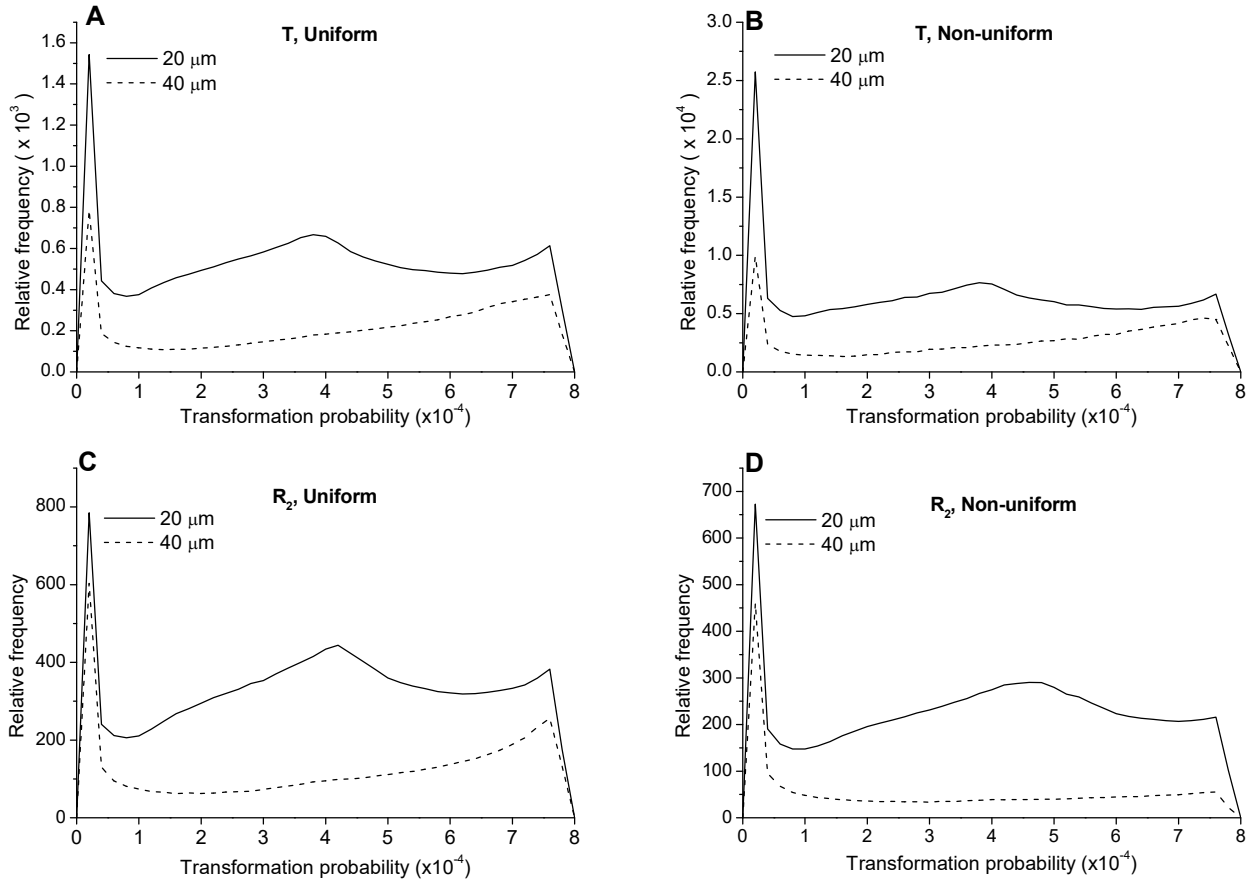
A
T, Uniform
20 μm
40 μm
Relative frequency (x 10^3)
Transformation probability (x10^-4)
B
T, Non-uniform
20 μm
40 μm
Relative frequency (x 10^4)
Transformation probability (x10^-4)
C
R2, Uniform
20 μm
40 μm
Relative frequency
Transformation probability (x10^-4)
D
R2, Non-uniform
20 μm
40 μm
Relative frequency
Transformation probability (x10^-4)

Figure 8

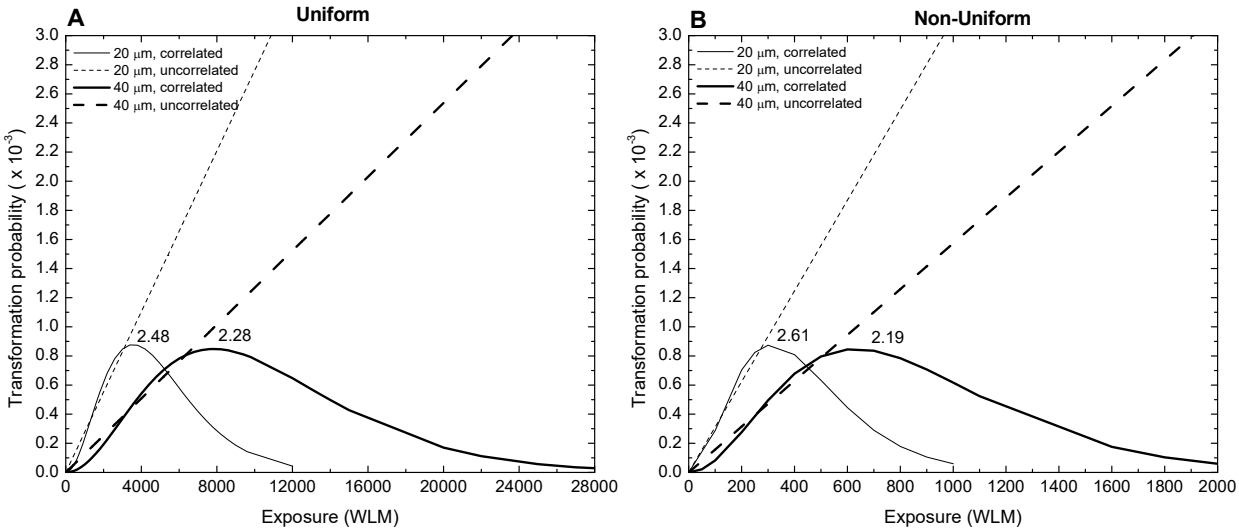
A
Uniform
20 μm, correlated
20 μm, uncorrelated
40 μm, correlated
40 μm, uncorrelated
Transformation probability (x 10-3)
Exposure (WLM)
2.48
2.28
B
Non-Uniform
2.61
2.19